International Journal of Neural Systems, Vol. 11, No. 2 (2001) 101–124

PERCEPTION OF ODORS BY A NONLINEAR MODEL OF THE OLFACTORY BULB

MICHAEL BREAKSPEAR*
Department of Mathematics and Statistics, University of Surrey, Guildford CU2 7XH, UK
Brain Dynamics Centre, Westmead Hospital, Sydney, NSW 2145, Australia
Department of Psychological Medicine, Faculty of Medicine, University of Sydney, NSW 2006, Australia
Department of Theoretical Physics, University of Sydney, NSW 2006, Australia
E-mail: mbreak@physics.usyd.edu.au

Received 27 October 2000
Accepted 6 March 2001

The behavior of the olfactory bulb is modeled as a network of interconnected cells with nonlinear dynamics. External inputs from sensory neurons are introduced as perturbations to subsets of cells within the network. We describe the attractors of the system and show how they can be classified and ordered according to their varying degrees of symmetry. By studying networks of attractors in the system's phase space, it is shown how different perturbations may evoke specific switches between various patterns of behavior. This ensures that different odors, even if present at extremely low concentrations, are able to evoke a specific spatio-temporal behavior in the olfactory bulb, permitting their unique perception. The model incorporates many of the processes proposed to mediate perception, such as the topographic organisation of sensory systems, destabilization of cortex by sensory input and synchronisation between neurons. It is also consistent with the character of the olfactory electroencephalogram.

1. Introduction

The perception of sensory stimuli constitutes one of the basic functions of neural systems. Theoretically, one is interested in how a multitude of different sensory stimuli can each lead to unique dynamical patterns in the neural systems which receive them. This problem is even more interesting when it is recalled that perceptions, such as smells, may be reliably triggered by microscopic sensory stimuli. Ideally, a model should also explain the features of experimental signals such as EEG. Clinically it is hoped that the study of these processes may elucidate pathological mechanisms leading, for example, to sensory hallucinations. In this paper we focus on the olfactory system, as this has been extensively studied.[1–3] We discuss a theoretical model of olfactory perception with experimental and clinical perspectives.

1.1. *Structure and function of the olfactory bulb*

One of the remarkable features of the olfactory system is its ability to reliably detect and discriminate between tens of thousands of odors at concentrations as low as a few parts per trillion (10^{12}). To begin with, odorant molecules attach to odor-specific membrane receptors in sensory cells of the nasal mucosa. This causes a conformal change in the receptor which leads to depolarization of the neighboring membrane.[4] As the distribution of different receptors is confined to small populations of

*Address after November 20, 2000: Department of Psychological Medicine, Westmead Hospital, Sydney, NSW 2145 Australia.

neurons,[2] specific odors lead to excitation of specific subsets of sensory neurons. These neurons project through the cribiform plate of the skull and form synaptic connections with mitral and tufted neurons in the highly interconnected olfactory bulb. The local circuitry of the olfactory bulb is constituted by dense inhibitory and excitatory interconnections and plays a critical role in processing incoming olfactory information before projecting to neurons in the olfactory cortex and other brain regions.[2,3] This paper examines the dynamics of the olfactory bulb during the cycle of odor-inhalation and exhalation.

1.2. *Dynamical behavior of the olfactory bulb during inhalation-exhalation*

Detailed analysis of 64-channel EEG recorded over the olfactory bulb indicates a characteristic pattern of activity during this cycle.[5–7] During exhalation, the EEG displays a low-amplitude, irregular signal with little coherence between different EEG channels. Time series analysis of this signal using the Grassberger–Procaccia algorithm yields a non-integer correlation dimension,[5] indicating that the underlying behavior may be governed by chaotic dynamics. During the inhalation of a *familiar* odor, the EEG changes quickly to a high-amplitude signal with an almost-periodic waveform and high coherence between channels. The amplitude of this waveform differs between EEG channels so as to form a specific spatial pattern for each specific odor.[6] Inhalation of a *novel* odor does not produce an almost-periodic signal. The EEG retains the irregular and discordant pattern of the exhalation signal. Any novel odor, however, can be learned through repeated exposure and reinforcement, whereupon the EEG evoked by its inhalation becomes almost-periodic, with a new unique amplitude distribution.[7]

This pattern of activity lends itself to the following interpretation.[8–10] Firstly, the olfactory bulb plays a critical role in creating dynamical representations of learned odors by constructing coherent structures for interpretation by the olfactory cortex and other brain regions. The pattern of activity that plays this role is a robust, almost-periodic signal with a characteristic amplitude distribution for each odor. In this way, the entire bulb is involved in producing a dynamical structure — a spatio-temporal attractor — in response to an odor.

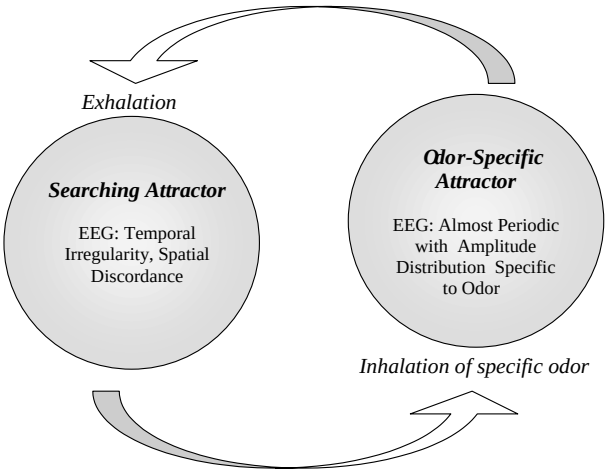

Fig. 1. Representation of olfactory bulb dynamics during cycle of inspiration-expiration. Lower arrow shows switching of bulbar dynamics following inhalation of a familiar odor. Top arrow shows reinstatement of searching attractor during expiration.

During exhalation, the activity of the olfactory bulb is governed by a "searching attractor" with a spatially discordant and temporally chaotic waveform. This attractor appears reliably during exhalation, but switches quickly to one of many possible odor-specific attractors following even nanoscopic sensory perturbation. This cycle of inhalation-exhalation dynamics is summarised in Fig. 1.

1.3. *Aims and structure of this paper*

We are thus left with an intriguing but seemingly elusive dynamical problem: How to describe a chaotic spatio-temporal attractor that appears reliably during exhalation but is at the same time very close to a large number of other attractors. Additionally, how do small but specific sensory perturbations cause specific jumps from the former attractor to one of the latter? In this paper, we model the behavior of the olfactory bulb as an ensemble of globally coupled cells with nonlinear responses. We show that the structure of attractors and their basins of attraction in this system permit an explanation of these phenomena. Our approach is motivated by a proposal of Kaneko in his study of attractors in high-dimensional systems with symmetry.[11–13] Specifically, he has proposed that this searching attractor must have a large basin of

attraction that is nonetheless "riddled" with the basins of other attractors. These are attractors in the sense of Milnor[14] and are defined below. We review this proposal and demonstrate how the anisotropic character of the basin riddling permits specific switching between attractors depending on specific types of perturbation.

The paper is structured as follows. In Sec. 2 we model the dynamics of the olfactory bulb as a globally coupled nonlinear map (GCM) with topographically organised sensory input. In Sec. 3, we review the appearance of coherent clusters and attractors in these globally coupled maps. We define Milnor attractors and basin riddling and show that these appear robustly in GCMs. A group-theoretic ordering of attractors, based on their symmetries, is introduced. This permits orbits to be "tracked" from typical random initial conditions to attractors. In Sec. 4, the transverse Lyapunov exponents are defined, and the structure of phase space is examined more closely. This allows a demonstration of how different sensory perturbations are associated with specific probabilities in the jumps between different attractors. In Sec. 5, the relationship between these dynamics and the EEG signals recorded from the olfactory bulb is discussed. Mechanisms for olfactory hallucinations, which are seen in some forms of epilepsy as well as schizophrenia and drug-induced psychoses are also proposed. In Sec. 6, the strengths and limitations of the present model are discussed in comparison to others in the literature.

2. The Olfactory Bulb as a Globally Coupled Map with Sensory Perturbations

In this section we model the olfactory bulb as a network of interconnected cells with nonlinear dynamics. Sensory input from the nasal mucosa and neuromodulatory inputs from other regions of the brain (such as monoamine pathways and limbic structures) are introduced.

2.1. *Modeling local dynamics within the olfactory bulb*

Sensory neurons from the olfactory mucosa synapse with mitral cells in the olfactory bulb. The synapses occur in structures known as glomeruli, which contain about one hundred mitral cells. Mitral cells, together with tufted cells are the main excitatory neurons of the olfactory bulb, and form dense and mutual connections with periglomerular and granule cells, which are inhibitory. The structure of the glomeruli, together with the local connectivity of the inhibitory neurons, confers a modular structure on the olfactory bulb[1] which we will take as the basic functional unit of our model. These modules are analogous to the microcolumns found in the neocortex.[15]

One of the difficulties modeling the dynamics of a neural system derives from the very large number of neurons involved. To counter this problem, the mass action of thousands of neurons averaged together is often studied.[16] The effect of averaging is to smear the all-or-nothing threshold potential of individual neurons into a sigmoid relationship between local mean dendritic potential and local mean firing rate.[17] Thus we consider the local mean firing rate of the excitatory neurons, $x(t)$, and inhibitory neurons, $y(t)$ in the locale of each glomerulus. The firing rates are normalized such that maximum firing occurs with $x(t)$ or $y(t) = 1$. Thus each range in the interval $I = [0, 1]$. Furthermore, we assume the average membrane potential is determined by excitatory and inhibitory impulses that each neuron receives. Thus, in one of these olfactory modules,

$$\begin{pmatrix} x(t+1) = \sigma_u(\omega_{ee}x(t) + \omega y_{ie}(t)) \\ y(t+1) = \sigma_u(\omega_{ei}x(t) + \omega_{ii}y(t)) \end{pmatrix} \equiv F_u \begin{pmatrix} x(t) \\ y(t) \end{pmatrix} \tag{1}$$

where,

$$\sigma_u(z) = \frac{1}{1 + e^{-uz}}, \tag{2}$$

is the neural activation function of sigmoid type. The parameter, $u > 0$, controls the responsiveness, or *gain*, of all neurons in the node to an input. This parameter models input to the bulb from other brain regions, modifying the state of arousal, such as during hunger or fear. The connection matrix, $W = w_{kk}$, represents the strength of local excitatory-inhibitory neural interactions. For any given matrix W, the network in (1) defines a one-parameter family of iterations of the map F_u on $I^2 = [0, 1] \times [0, 1]$. It can be shown[18] that when W takes the form,

$$W = \begin{bmatrix} a & -ka \\ b & -kb \end{bmatrix}, \tag{3}$$

with a, b, $k > 0$, then F_u is a diffeomorphism, and is topologically conjugate to the one-dimensional map,

$$f_u(x) = \sigma_u(ax) - k\sigma_u(bx)\,. \tag{4}$$

This map, which is known as the Wang-oscillator,[19] allows one to draw upon the robust results derived from studies of one-dimensional maps. Furthermore, when $k = 1$, and $a \geq 2b$, then g_u (and hence F_u) is topologically conjugate to a *full family* of *S-unimodal maps on the interval* [0,1]. This result,[18] which requires a single maximum and restricts the types of points of inflexion that are permitted, is important because these are the most widely studied and best understood one-dimensional maps.[20,21] They exhibit the period-doubling route to chaos with increasing u. In addition, when the map is in the chaotic regime, unstable periodic orbits are dense amongst the attractors, a result which is of particular significance in our later analysis. The best known example of this class of equations is the logistic map,

$$f_u(x) = 1 - ux^2\,. \tag{5}$$

Thus for quite general connection weights it is possible to gain a complete understanding of the behavior of (1) by studying (4) and (5).

2.2. *Coupling of local nodes to model global olfactory bulb dynamics*

The large-scale structure of the olfactory bulb is modeled by coupling these individual nodes into a complex assembly. We initially consider global, symmetric coupling between all nodes, although the effect of lessening these constraints will also be considered. The coupling is mediated by synaptic connections between mitral cells, which are the principle long-range excitatory neurons of the olfactory bulb. Hence we consider the evolution of the state space vector $X = (x_1, x_2, \ldots, x_n)$ in N-dimensional Euclidean space, R^N by the system,

$$X(t+1) = G_{u,c}(X(t))\,, \tag{6}$$

where G is defined by,

$$x_i(t+1) = (1-c)f_u(x_i(t)) + \sum_{j=1}^{N} \frac{c}{N}.f_u(x_j(t))\,. \tag{7}$$

The variable $x_i(t)$ describes the mean rate of cell firing of the ith node in the assembly at time t and N is the total number of nodes considered. The function $f_u(x_i)$ describes the response characteristics of each individual node by either (4) or (5). The parameter $c \in [0,1]$ represents the strength of coupling between nodes. It can be seen that with no coupling ($c = 0$) the nodes evolve independently and there is no collective behavior. With maximum coupling ($c = 1$) all the nodes follow the same evolution and thus synchronise after one time-step. Between these extremes, the behavior can be quite complex, with clustering, chaotic synchronisation and the emergence of long temporal scales,[22–24] as examined below. In the olfactory bulb, as in other brain regions, the strength of coupling between cells is modulated by diffusely projecting monoamine neurons from brain stem structures, principally the dorsal raphe nucleus.[25]

In this paper, we are interested in both the transient and asymptotic behavior of G. To study this explicitly, the following definitions are recalled.[26] Suppose we have a map, G, and a manifold R^N such that $G : R^N \to R^N$. An *orbit* is a sequence of iterates $\{X_n\}_{n\in Z}$ with initial condition, $X_0 \in R^N$ and nth iterate $G^n(X_0) = X_n$. For any orbit,

$$\omega(X) = \bigcap_{N>0} \overline{\bigcup_{n>N} X_n}$$

is the *ω-limit set*. This is the asymptotic behavior of a specific initial condition. Given any compact invariant set A, then we define its *basin of attraction*,

$$B(A) = \{X \in M : \omega(X) \subseteq A\}\,.$$

An *invariant* set satisfies $F(A) \subseteq A$. A compact invariant set is said to be an *attractor* if it has a basin of attraction with positive (Lebesgue) measure in R^N. This is motivated by the intuitive definition of an attractor as "the set of points to which most points evolve under iterates of G"[14,20] — the long-term behavior of a large set of initial conditions. An attractor, A, is said to be *asymptotically stable* if the time evolution of G returns to A following any small perturbation of any orbit. That is, for all $X \in A$ there exists some $\delta > 0$ such that $|X-Y| < \delta$ implies $\omega(Y) \subseteq A$ and for all $\varepsilon > 0$ there exists $\delta > 0$ such that $X \in B_\delta(A)$ implies $G^n(X) \in B_\varepsilon(A)$ for all n. An attractor is said to be *structurally stable* if it persists despite any small perturbation to the function

G itself. Otherwise it is said to be *fragile*.[27] These important two stability properties are quite different, and certainly are not satisfied by all attractors.

At this stage, we note that Eq. (6) is highly symmetrical. By this, we mean that there exists a group of transformations, Γ, such that $\gamma G(X) = G(\gamma X)$ for any $\gamma \in \Gamma$. It is straightforward to see that this is true where γ denotes any permutation of the subscripts of the indices of X. The set of all such permutations constitutes the symmetric group, S_N.

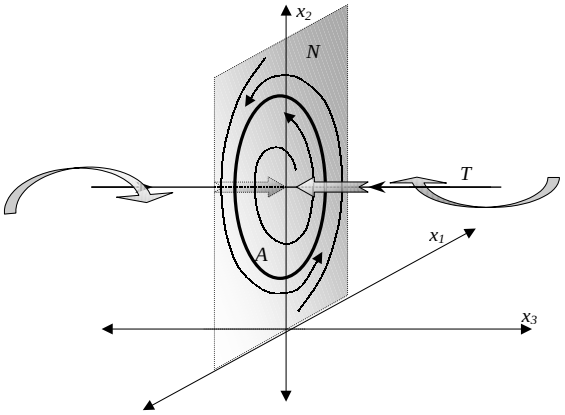

(a)

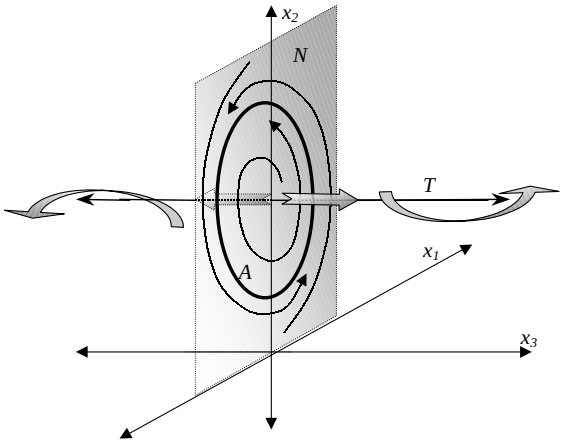

(b)

Fig. 2. Phase space diagram illustrating transverse stability for hypothetical flow with periodic orbit A, embedded in invariant manifold N. A is an attractor of the system confined to N, as illustrated by the thin arrows in the plane. (a) A is also attracting in the transverse direction T, as illustrated by the ribbon arrows, and so is an asymptotically stable attractor in the full phase space. (b) A is transversely unstable, and so is a saddle in the full phase space.

A related property is that the linear manifolds of the form $\{x_i = x_j = \cdots = x_k\}$ for $i, j, k \in (1, 2, \ldots, N)$ are invariant under the action of G. That is, any orbit that starts on one of these manifolds remains there for all time. These *invariant manifolds* may contain attractors, saddles, or repellors depending on the attraction or repulsion of orbits in the direction *transverse* to the manifold.

The importance of transverse stability is illustrated in Fig. 2. which shows a hypothetical example of an attracting periodic orbit in the invariant plane $(x_1 = x_2)$. In Fig. 2(a), this orbit is also attracting in the transverse direction and is thus an attractor in the full phase space. In Fig. 2(b), the same orbit is transversely repelling, and is thus a saddle in the full phase space. It is a *transversely unstable* period-1 orbit.

2.3. *Sensory perturbation and perception*

Sensory input is introduced by perturbing a subset of the nodes over a single time-step, or over a sequence of time-steps. Let S be the set of all learned odorant molecules. We define a bijective mapping $h : S \to X$ that associates with each odor, s, a subset of nodes in the network; $h(s) = (x_a, x_b, \ldots, x_c)$ where $a, b, \ldots, c \in (1, 2, \ldots, n)$. This captures the diffuse, although topographically restricted nature of sensory projections from olfactory mucosa to glomeruli. A sensory perturbation is then modeled by the addition of a small random term to each of these nodes during a finite sequence of iterations, representing excitation of the cells by afferent input. That is, for $t \in [t_1, t_2, \ldots, t_f]$ and an inhaled odor $s \in S$,

$$x_i(t+1) = (1-c) f_u(x_i(t)) + \sum_{j=1}^{N} \frac{c}{N} \cdot f_u(x_i(t)) + \delta . rand_i(t) \chi_i^{h(s)} \tag{8}$$

where δ is the (arbitrarily small) amplitude of the sensory perturbation, $rand_i$ is an independent random number with uniform distribution across the interval $[-0.5, 0.5]$ and,

$$\chi_i^{h(s)} = \begin{cases} 1 & \text{if } x_i \in h(s) \\ 0 & \text{if } x_i \notin h(s) \,. \end{cases}$$

Before and after this "inhalation" sequence, the system evolves according to (6). Transients evoked

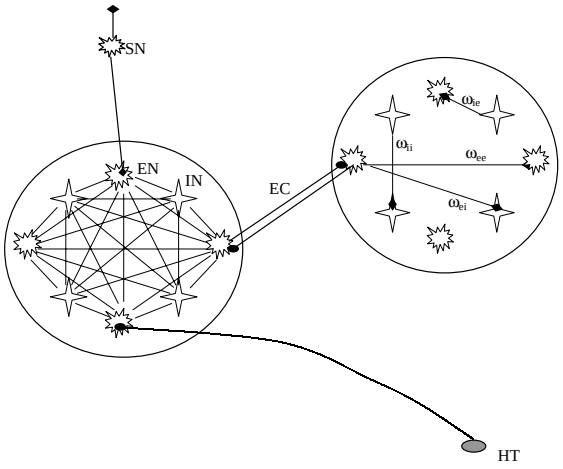

(a)

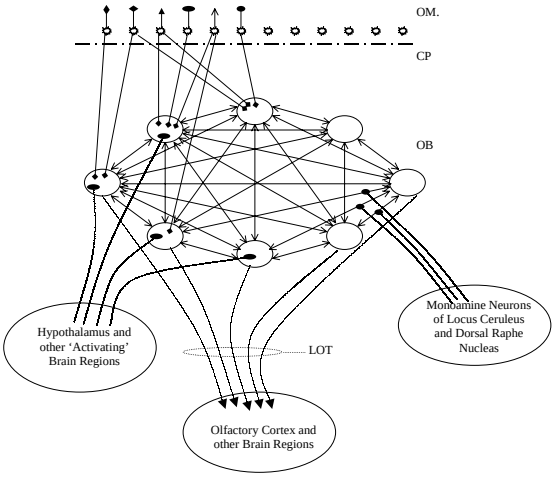

(b)

Fig. 3. Schematic diagram of the present model. (a) Sensory neurons (SN) project to excitatory neurons (EN) such as mitral cells in the bulb. These form dense local reciprocal connections with other excitatory cells, including tufted cells, and inhibitory neurons (IN) such as periglomerular and granule cells. The strengths of these connections are parameterised by the connection matrix w_{ee} etc. The gain of the cells is modified by neurons projecting from other brain regions, such as the hypothalamus (HT). Connections between the local nodes are mediated by longer-range excitatory connections (EC). (b) On a larger scale the nodes are coupled together into an ensemble to constitute the olfactory bulb. Sensory neurons with different receptor populations in the olfactory mucosa (OM) project through the cribriform plate (CP) to the bulb (OB). Reciprocal coupling strength between nodes is modulated by monoamine neurons from brain stem nuclei. Excitatory neurons then project from the bulb via the lateral olfactory tract (LOT) to other brain regions.

by the perturbation are allowed to settle and the system again returns toward an attractor. We will say that the system has *perceived* the odor, s, when the perturbation sequence (7) evokes a jump from one attractor to another. Of particular interest in the current setting will be the attractors with large basins of attraction which nonetheless permit jumps onto another attractor following arbitrarily small sensory perturbations, thus modeling perception of extremely low concentrations of odorant molecules.

The structure of our model for the olfactory cortex is summarised in Fig. 3.

3. Spontaneous Activity of the Olfactory Bulb

In this section we examine the attractors, basins and stability properties of (6). These are motivated by numerical examples with random initial conditions, where the logistic map (5) is substituted into (6). The attractors represent the spontaneous, or resting activity in the olfactory bulb, in the absence of sensory stimuli. For simplicity, examples are illustrated for $N = 8$ nodes. Many more nodes than this are required to model the olfactory bulb. However, similar behavior is observed[12] with $N > 100$. Numerical simulations were carried out in MatLab, using double-precision arithmetic.

3.1. *Attractors, basins and stability of the model*

To begin, suppose $c = 0.12$ and $u = 0.9$. In this case, all individual nodes rapidly synchronise and the system exhibits coherent periodic behavior. That is, there is rapid collapse onto a period-2 attractor embedded in the one-dimensional manifold, $x_1 = x_2 = \cdots = x_8$ (the *hyperdiagonal*). The coupling is of sufficient strength to produce contraction of the initial eight degrees of freedom, producing a single coherent cluster with only one degree of freedom. Note that any two subscripts denoting node position can be permuted without disturbing the structure of the attractor.

Alternatively, if $c = 0.12$ and $u = 1.8$, all individual nodes display chaotic behavior and do not synchronise. Therefore the attractor for the system spans all eight dimensions (R^8) and is chaotic in each direction. Because of the asymmetry of the chaotic

behavior (which derives from the random distribution of initial conditions) $x_1 \neq x_2 \neq \cdots \neq x_8$ for all t. Thus no two individual nodes can be permuted.

Kaneko refers to these two types of behavior as the *coherent phase* and *turbulent phase*[12] respectively. They represent the extremes of regularity and symmetry versus discordance. However the attractors in both these cases share the same stability properties. They both persist in large open regions of parameter phase (the former with small u or large c, and the latter for large u or small c). Hence they both are structurally stable. Additionally, they attract all conditions. Thus, following any perturbation of the dependant variables, the system always returns to the same attractor. Following Kaneko,[12] we perturb all dependant variables by a random amount of average amplitude δ for one timestep and define $P_R(\delta)$ as the probability that the system returns to the same attractor subsequent to the perturbation. Trivially in this case $P_R(\delta) = 1$ for all δ and in particular,

$$\lim_{\delta \to 0^+} P_R(\delta) = P_R(0^+) = 1\,. \tag{9}$$

These attractors are thus asymptotically stable and structurally stable.

If u is increased smoothly from 0.9 and c held constant at 0.12, one observes the bifurcation from the coherent phase to the *partially ordered phase*.[12] The phase space in this parameter region is partitioned into several basins of attraction, each of which contains periodic attractors with 2 or 3 coherent clusters. The first to appear (at $u \cong 0.96$) are the attractors with 2 coherent clusters each with 4 synchronised nodes. 2-cluster periodic attractors with disparate cluster sizes then appear — first those with clusters of 5 and 3 nodes ($u \cong 1.08$), then those with clusters of 6 and 2 nodes ($u \cong 1.18$) then those with a cluster of 7 nodes and a single unsynchronised node ($u \cong 1.28$). All of these attractors have period-2 and all are stable to small perturbations of their dependent variables; $P_R(0^+) = 1$. That is, although the phase space is partitioned into different basins of attraction, each basin is open and hence the attractors are asymptotically stable. These attractors are also structurally stable. At $u \cong 1.30$, attractors with 3 disparate clusters of synchronised nodes are also seen, such as those with a cluster of 4 nodes and 2 clusters with 2 nodes each. The appearance of each of these attractors with increasing u is shown in Fig. 4.

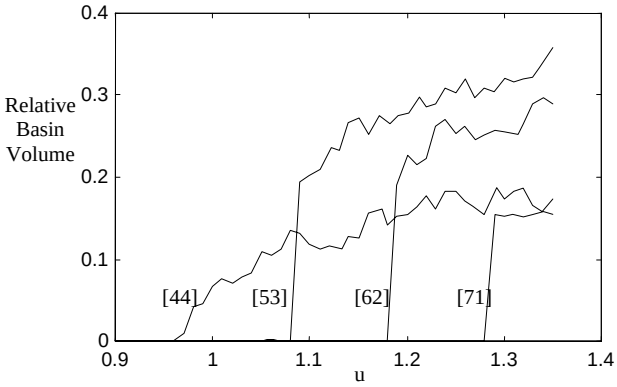

Fig. 4. Consecutive appearance of attractors with two unsynchronised clusters in the partially ordered phase with $N = 8$ and $c = 0.12$. See main text for attractor coding. Vertical axis is relative basin volume of each attractor, obtained from uniformly distributed random initial conditions for each node on the interval $[-1, 1]$. Total volume has been normalized to 1. Only the basin for the completely coherent attractor [8] has been omitted. This is the only attractor if $u < 0.96$.

The nodes within each cluster (e.g., x_i, x_j, x_k) have the same time evolution. Thus the orbits are confined to the invariant manifold, $x_i = x_j = x_k$. The attractor lies along the intersection of the invariant manifolds containing each synchronised cluster.

As u is increased further, attractors with greater numbers of coherent clusters appear, and there exists period-doubling bifurcations for each attractor. The onset of chaotic temporal behavior heralds the appearance of the *complex ordered phase*[12] at $u \cong 1.43$. There are several features of this region:

1. The phase space is partitioned into many basins of attraction. In Fig. 5 is shown the number of different types of attractors for different values of u. This number peaks in the complex ordered phase.
2. Attractors with small numbers of synchronised clusters and several unsynchronised appear in large numbers.
3. The temporal behavior of the attractors becomes quite complex. In addition to periodic and chaotic behavior, one observes bursting between synchronised and desynchronised

behavior and complex irregular switching between bursting behavior and almost periodic behavior. This is discussed further below.

4. There are attractors with chaotic evolution which become periodic following small changes to either parameters. These attractors are thus fragile. It has been conjectured[28] that chaotic attractors with m positive Lyapunov exponents can be dispelled by small changes to $n \geq m$ parameters. In the present setting, since there are 2 control parameters, this corresponds to attractors with 1 or 2 chaotic clusters. Attractors with 3 chaotic clusters remain structurally stable.
5. Attractors lose asymptotic stability. That is, small perturbations of the dependant variables (while the parameters are held constant) have a finite probability of causing the system to jump to another attractor. Thus $P_R(0^+) < 1$.
6. Chaotic saddles appear. These are invariant chaotic sets which attract in some transverse directions, but repel in others. Hence, in theory, $P_R(0^+) = 0$. With finite-precision arithmetic, however, these chaotic saddles occasionally "capture" orbits due to rounding off and calculations erroneously yield $P_R(0^+) > 0$. For this reason, they have also been termed "pseudo-attractors".[12,22]

As u is increased further, attractors with one small synchronised cluster and many unsynchronised nodes dominate phase space. This is shown in Fig. 6. Other attractors undergo transition to chaotic saddles. Eventually, at $u \cong 1.74$, all attractors other than the completely desynchronised state become saddles or repellors, and the turbulent phase is reached.

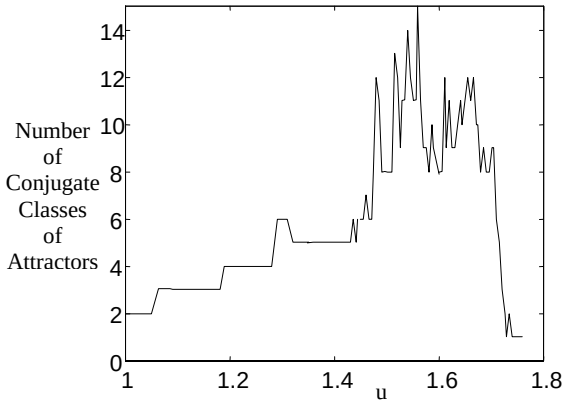

Fig. 5. Number of different conjugate classes of attractors with $N = 8$ and $c = 0.12$. See main text for definition of conjugate classes. Horizontal axis shows u increasing from the ordered to the turbulent phase.

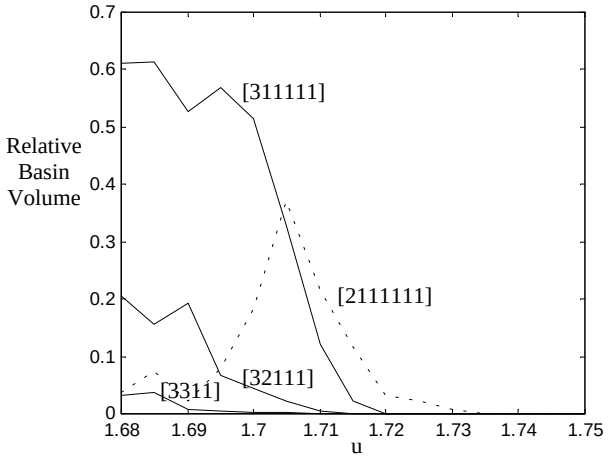

Fig. 6. Relative basin volume for attractors with increasingly small and numerous clusters in the transition from the complex-ordered to the turbulent phase. Axis and methods as per Fig. 4. Only the basin for the completely desynchronised attractor $[1^8]$ has been omitted. This is the only attractor once $u > 1.735$.

3.2. *Riddled basin attractors*

Property 5 is of most significance in the current context, as this permits small sensory perturbations due to odor inhalation to cause a sudden switch in the bulbs spatio-temporal behavior. Attractors that are *not* asymptotically stable are attractors in the sense of Milnor.[14] The basins of these attractors are *riddled* with points that belong to another basin of attraction.[29] More formally, a basin is said to be riddled when any ball, no matter how small, centred on any point in the basin contains a set of positive (Lebesgue) measure of points belonging to other basins of attraction. That is, for all $x \in B(A)$ and all $\delta > 0$,

$$l(B_\delta(x) \cap B(A)) > 0 \quad \text{and} \quad l(B)\delta(x) \cap B^c(A)) > 0$$

where $l(.)$ denotes the Lebesgue measure on R^N. Thus riddled basins have no interior.[26] In the present context, the riddling arises from the unstable periodic points embedded in the synchronised chaotic

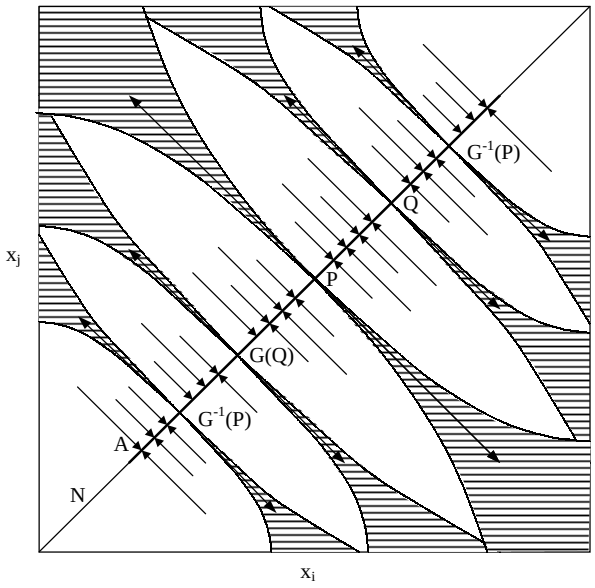

Fig. 7. Schematic representation of riddled basin attractor. A is contained within subspace N invariant under the action of G, $G(N) \subseteq N$. Unstable periodic points such as P (period-1) and Q (period-2) are repelling in the transverse direction. Also shown are two pre-images of P, $G^{-1}(P)$. The transversely unstable periodic orbits and their pre-images create narrow tongues of repelling regions, shaded. Other orbits are attractin towards the chaotic attractor contained within N. Here N corresponds to the cluster of synchronised nodes, $x_i = x_j$.

attractor which repel orbits in the direction transverse to the attractor.[23,30] These orbits create narrow tongues of repelling orbits. Any sensory perturbation that causes the system to land within one of these tongues permits a jump from one attractor to another. This is schematically depicted in Fig. 7. Because the set of repelling orbits have positive measure, there is always a finite probability of this occurring and hence $P_R(0^+) < 1$. Conversely, the basin of attraction also has positive measure so that $P_R(0^+) > 0$. Henceforth we refer to attractors with riddled basins as *riddled basin attractors*.

Typically, as u increases, so do the number of transversely unstable periodic points, and hence the measure of repelling obits in the neighborhood of A approaches one. Finally, $P_R(0^+) = 0$ as the attractor undergoes a *blowout bifurcation* to become a saddle.[31] This phenomenon is examined in more detail in Sec. 4.

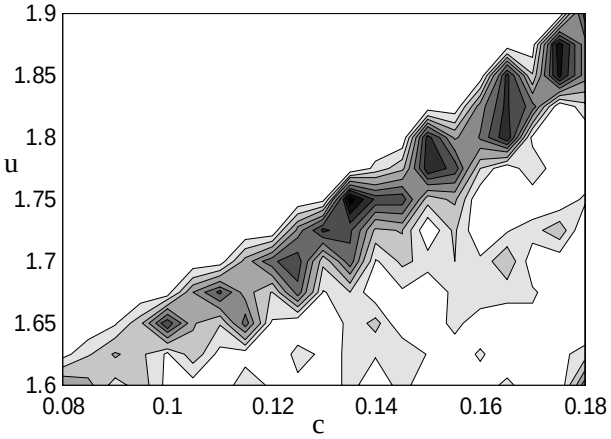

Fig. 8. Contour map showing relative distribution of riddled basin attractors in parameter space. Random initial conditions chosen as per Fig. 4. Contour shading shows percentage of initial conditions evolving toward riddled basin attractors. Increments are of 10% from minimum (white) 0–10%, to maximum.(black) 90–100%. Riddled basin attractors calculated numerically as satisfying $0 < P_R(0^+) < 1$.

The same transition from the coherent through the partially- and complex-ordered phases, to the turbulent phase also occurs if u is fixed (e.g., at 1.68) and c is *decreased*. Figure 8 depicts the proportion of initial conditions in parameter space limiting toward riddled basin attractors. The appearance of these attractors is robust, in that they occur in a large region of parameter space. Moreover, when they do appear, their basins of attraction typically are of large volume and dominate phase space. That is, whilst they are locally unstable, they are globally attracting.[12] This means that medium to high amplitude non-specific noise, which randomly samples phase space, preferentially selects the basins of riddled basin attractors.

Examples of all these behaviors are illustrated in Secs. 3.4 and 4.4.

3.3. *Coding and symmetry of attractors*

Attractors in these systems can be *classified*[12] by the number of clusters k and the number of elements for each cluster N_k. They can be *coded* by the clustering condition $[N_1 \geq N_2 \geq \cdots \geq N_k]$. Due to symmetry, there can be many attractors with the same code. In the coherent phase there is a single attractor with code [8], whilst in the partially ordered phase,

there are multiple attractors each with codes [4,4], [5,3], [6,2], [7,1], [4,2,2] or [4,3,1] etc., In the turbulent phase there is again one attractor, with code $[1,1,1,1,1,1,1,1] = [1^8]$.

It is also possible to classify and order attractors by exploiting the symmetry of G. Consider the single attractor in the coherent phase. Because the time evolution of all nodes is identical, the state space vector is not affected by any permutation of indices between nodes. Thus, like G itself, this attractor is invariant under the action of the symmetry group S_8. In the partially ordered and complex ordered phases, the attractors are preserved if the permutations are only between nodes within the same clusters. In other words, for any attractor with clusters of synchronised nodes there exists a subgroup of S_8 whose action preserves the structure of the attractor. For the coherent attractor, this subgroup is the whole group. For the turbulent attractor it contains only the identity element. Using the notation of Ashwin[32] we now develop the method of classifying and ordering the attractors according to their symmetries. A brief review of the prerequisite group theoretic concepts is presented in Appendix I.

Consider the action of a group Γ on the manifold R^N given by $X \to \gamma X$ for $X \in R^N$ and $\gamma \in \Gamma$. The *isotropy subgroup* of a point X, denoted $\Sigma(X)$ is the subgroup which fixes the point X. Thus,

$$\Sigma(X) = \{\gamma \in \Gamma : \gamma X = X\}\,.$$

$\Sigma(X)$ describes the symmetry of the point X. We refer to isotropy subgroups up to conjugacy. Recall that all points on the attractor must have the same symmetry. Hence we define the *fixed-point subspace* of the isotropy subgroup Σ as the set of all points in R^N which are invariant under the action of Σ,

$$\mathrm{fix}(\Sigma) = \{Y \in R^N : \sigma Y = Y \quad \text{for all } \sigma \in \Sigma\}\,.$$

and thus have the same symmetry as X. In the present context the group Γ is the symmetry group S_8 where each element is a specific permutation of the subscripts of the state space vector, X. The fixed-point subspaces are precisely the invariant manifolds of G. Because attractors lie on the intersection of these manifolds, they can be classified according to the subgroup for which this intersection is the fixed-point subspace. For example the attractor with the code [3221] lies on the invariant manifold fixed by the subgroup $S_3 \times S_2 \times S_2 \times S_1$. Note that there are in general many subgroups in each conjugacy class. Each specific subgroup describes the symmetry of a specific attractor, and the conjugacy class captures the shared symmetry of all attractors with the same code. We will refer to such attractors as *conjugate*. Even with $N = 10$ there are tens of thousands of conjugate attractors in the complex-ordered phase. This exaggerates the peak in the number of attractors for the complex phase, as shown in Fig. 5, by several orders of magnitude.

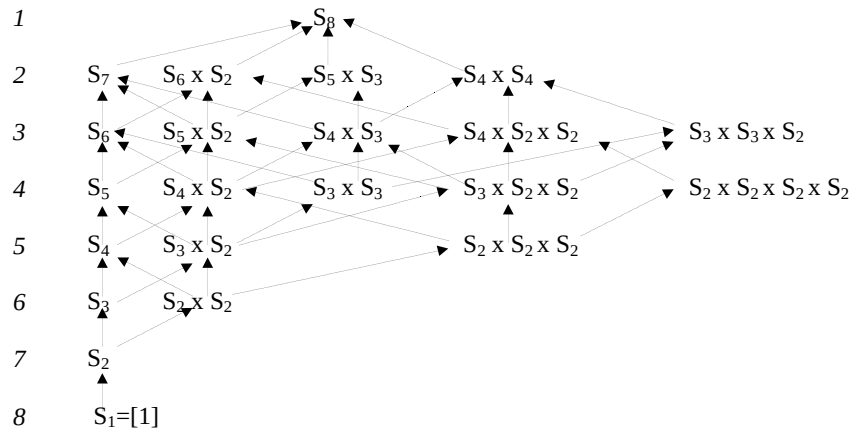

Fig. 9. The lattice of isotropy subgroups of S_8. Arrows depict containment (increasing symmetry). The numbers in the column correspond to the degrees of freedom in the fixed-point subspaces of all subgroups in each row.

There also exists a partial ordering of the isotropy subgroups, the *isotropy lattice*, given by $\Sigma_1 < \Sigma_2$ if there exists $\gamma \in \Gamma$ such that $\gamma^{-1}\Sigma_1\gamma$ is a proper subgroup of Σ_2. This permits a rigorous ordering of the attractors of (6), as shown in Fig. 9. It provides a formal structure for the bifurcation diagram of the olfactory bulb as depicted in Fig. 13 of [33]. The descending row numbers, as labelled in Fig. 9, correspond to the number of degrees of freedom in the fixed point subspaces of each row. As we shall see below, the isotropy lattice also shows us exactly which jumps between attractors are possible consequent to sensory perturbation.

3.4. *Numerical examples of attractors and saddles*

In this section we start with random initial conditions and chart the subsequent orbit on the isotropy lattice. Due to the generic inequality of the random initial conditions, the initial state vector has only the trivial symmetry of the subgroup S_1. The ω-limit set of each initial condition is reached only in the limit as $t \to \infty$. However, in the numerical calculations, there is an artificial jump onto the attractor after only a finite number of iterations due to rounding off. Fortuitously, this allows us to identify not only the attractor, but also the transient path *en-route*. This path can be charted on the isotropy lattice. Each step up the lattice occurs when a node synchronises with another, or fuses with a cluster of nodes. This corresponds to the absorption of the orbit into an invariant subspace of progressively increasing symmetry, and the consequent loss of one degree of freedom. Spontaneous descent down the lattice is not possible.

In Fig. 10(a) is charted the progress of some typical orbits in the coherent phase. Although the ω-limit set inevitably has the symmetry of the group S_8, several distinct paths through phase space are possible. Typically there is a cascade of synchronisation involving one cluster with serial capture of individual nodes. Occasionally a smaller cluster also appears, and fuses with the larger cluster at the final stage. Fusion of two large clusters is not observed.

Analogous paths are charted in Fig. 10(b) for the partially-ordered phase. Note the parallel fusion of two or three clusters of comparable size is seen. This accounts for the overall shift of paths to the right of the lattice. Occasionally clusters fuse *en route* to the fully synchronised attractor. As u increases, the orbits halt their progression at stages of partial symmetry. This corresponds to the appearance of basins of attraction for partially synchronised attractors.

In the complex-ordered phase, Fig. 10(c), no paths reach the state of maximum symmetry. Indeed, some initial conditions maintain trivial symmetry for all time. As noted above, chaotic invariant sets with $P_R(0^+) = 0$ corresponding to chaotic saddles appear. However, orbits on attractors of lower symmetry often shadow these saddles for lengthy but irregular sequences of iterations. Such attractors, "stuck on" to invariant subspaces of higher symmetry have been described in other dynamical systems.[34] Sudden, irregular bursts away from these saddles occur whenever the orbit approaches transversely unstable periodic orbits. An example of this behavior is seen with $c = 0.12$ and $u = 1.683$ for attractors with $S_3 \times S_3$ symmetry, shadowing a chaotic saddle with $S_4 \times S_3$ symmetry. Occasionally this attractor even shadows a saddle with $S_4 \times S_4$ symmetry. This can be visualised on the lattice, by noting when the orbits are nearby (e.g., within 10^{-3} units) manifolds of higher symmetry. The dotted lines in Fig. 10(c) represent this shadowing of saddles.

Other complex behaviors are also possible. With $c = 0.12$ and $u = 1.68$, the attractor with $S_3 \times S_3$ symmetry continues to intermittently shadow the chaotic saddle with $S_4 \times S_3$ symmetry. However, the intermittent bursts are occasionally captured by lengthy epochs of period-4 like behavior. The system switches between these two types of behavior at irregular intervals. Figure 11 examines an example of this attractor. Node x_1 is in one of the clusters of three synchronised nodes; x_2 is not synchronised with any other node. Figure 11(a) shows the time evolution of the Euclidean separation, $d = x_1 - x_2$. The block of regular behavior between the arrows is clearly different from the otherwise very irregular timeseries. In Fig. 11(b) is shown the attractor in phase space during the irregular behavior. It can be seen that during this time the attractor is stuck onto the invariant manifold over higher symmetry (fixed by $S_4 \times S_3$), $x_1 = x_2$. In fact, the attractor is shadowing a chaotic saddle, shown in Fig. 11(c), embedded in this manifold. Intermittent bursting

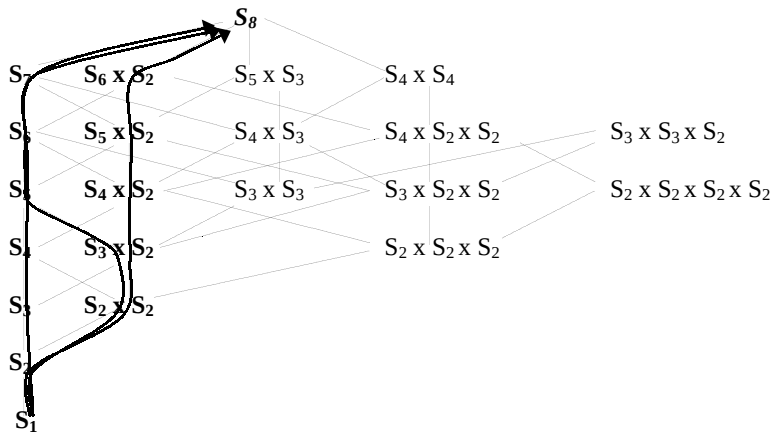

(a)

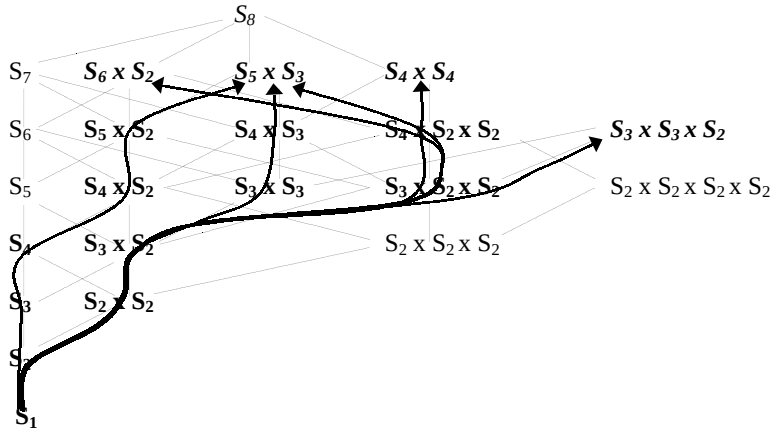

(b)

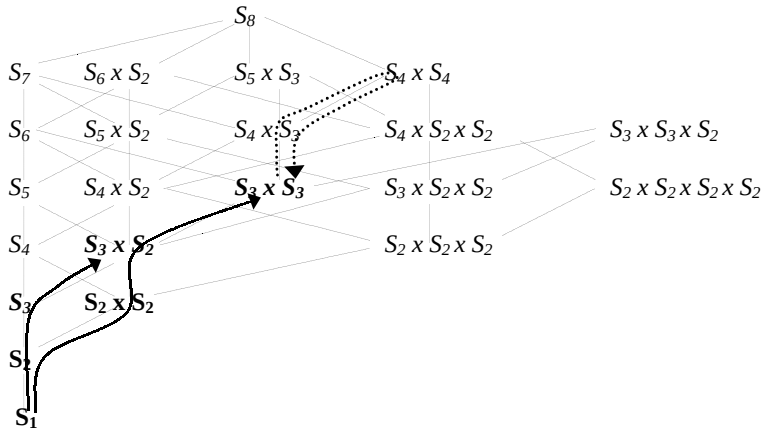

(c)

Fig. 10. (a) Typical orbits in the coherent phase, commencing with random initial conditions and evolving to the coherent structure. Arrows depict successive progress of the orbits onto fixed-point subspaces of increasing symmetry. Transients pass through fixed-point subspaces highlighted in bold. Subgroups highlighted in *bold italics* fix the subspace containing the attractor. (b) In the partially ordered phase, invariant sets of saddle-type appear. These are in subspaces fixed by the subgroups in *italics*. (c) In the complex-ordered phase, attractors fixed by subgroups towards the bottom of the lattice often shadow saddles above them on the lattice, depicted by the dotted arrows.

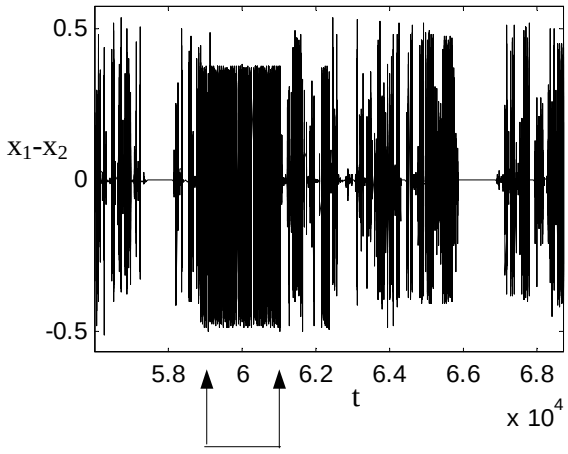

(a)

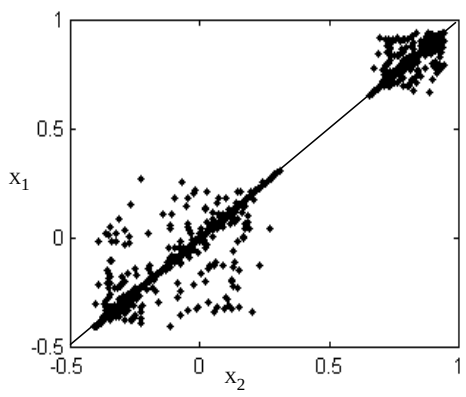

(b)

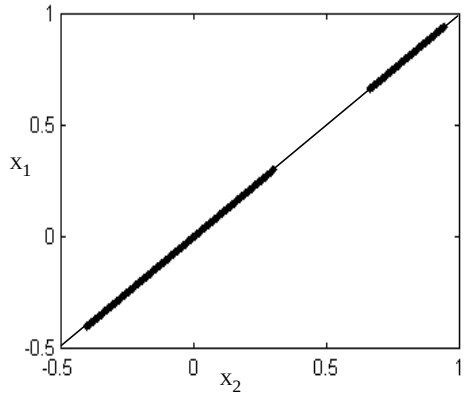

(c)

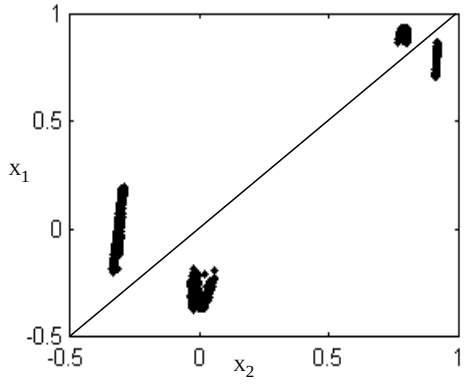

(d)

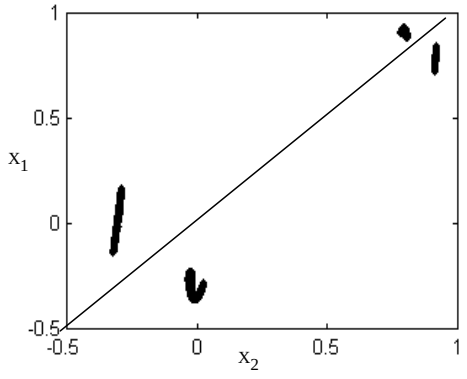

(e)

Fig. 11. (a) Numerical simulation of attractor with $S_3 \times S_3$ symmetry ($x_1 = x_3 = x_4$ and $x_5 = x_6 = x_7$). (a) Evolution of Euclidean distance between x_1 and x_2. Arrows delineate more regular block of behavior discussed in text. (b) Structure of the attractor in phase space during iterations *outside* of the delineated block. The diagonal corresponds to the invariant manifold with $x_1 = x_2$ fixed by $S_3 \times S_4$. (c) Chaotic saddle embedded within this invariant manifold which is shadowed by the attractor during epochs such as (b). The saddle is embedded in two disjoint intervals on this manifold. (d) Appearance of the attractor in phase space *during* the delineated block of (a). (e) Cluster of period-4 saddle orbits that are shadowed during epochs such as (d).

away from the saddle accounts for the scatter of points away from the diagonal in Fig. 11(b), and the irregularities in Fig. 11(a). One of these bursts has been captured by the regular behavior delineated by the arrows. Figure 11(d) reveals that during this block the attractor is confined to four small regions in phase space. In fact, the attractor shadows a large number of period-4 saddles embedded in these regions which are shown in Fig. 11(e). Thus the attractor spontaneously switches between two different semi-stable types of behavior.

In our model, all these types of behavior represent the spontaneous, or "resting" activity of the bulb. We include some of the more complex examples because they have implications for average measures of EEG activity. Spontaneous activity that explores several semi-stable types of behavior has no single typical behavior, or *archetype*. When computing dynamical measures of the system, it is necessary to use lengthy intervals in the time domain to ensure inclusion of all archetypes and hence adequate convergence to dynamical means. However, by averaging across different types of dynamics, one produces measures that are, of themselves, never expressed by the system of interest. In the spatial domain, this includes methods based on principle components analysis, and in the time domain, most of the numerical algorithms for characterising nonlinear timeseries. It may therefore be advantageous to employ methods of analysis capable of capturing and quantifying archetypes[35] in complex dynamical systems.

We now progress from spontaneous to sensory-evoked activity.

4. Sensory-Evoked Dynamics of the Bulb

We have defined perception as the process by which (possibly small) sensory input leads to switching between attractors for the dynamics of the olfactory bulb. In this section, we consider the type of switches that can be induced by different types of sensory perturbation. We show that various switches have different probabilities of occurring following different odors. This forms the basis for how specific odors can lead to specific perceptions. To this end, we progress from a study of the dynamics within invariant manifolds to the dynamics in the transverse direction.

4.1. *Fission and fusion of synchronised nodes by sensory perturbation*

Sensory input is introduced by perturbing a subset of nodes in the system away from an asymptotic ("resting") state through (7), and then allowing it to evolve again according to (6). In general,[12] such a perturbation may lead to:

1. *Fission* (splitting) of a synchronised node out of a synchronised cluster. In this case, the system steps down the isotropy lattice.
2. *Fusion* (union) of two clusters (or a cluster and a single node) to create a larger cluster, in which case the system steps up the isotropy lattice.
3. The swapping of a node (or nodes) between one cluster and another. This is actually a two-step process involving fission of an attractor into an unstable transient, which then evolves toward an attractor of higher symmetry. In this case, the new attractor is on the same level of the lattice, but has different subgroup symmetry. It is possible that the new attractor is conjugate to the previous one.

The effect of the perturbation depends critically upon the symmetry of the attractor and the subset of nodes perturbed. A perturbation involving a node in a synchronised cluster causes transient desynchronisation of that node. In the phase space, this corresponds to perturbing an orbit *transverse* to, and thus out of, an invariant manifold. If the perturbation is small and the attractor is asymptotically stable, then the orbit will evolve back to the invariant manifold and the odor will not have been perceived. However, if the attractor has a riddled basin there is a finite chance that the orbit will be kicked out of the basin, causing permanent desynchronisation of that node, fission of the attractor and thus perception of the odor. The probability of this occurring depends upon the density of the riddling in the direction of the perturbation. This density is typically anisotropic.[36]

Perturbations involving *only* unsynchronised nodes are tangent to the invariant manifolds which contain the attractor. Therefore, fission of clusters is not possible. However, fusion of nodes can occur if, (1) there is an invariant set of higher symmetry that is an attractor, and not a saddle or repellor; and (2)

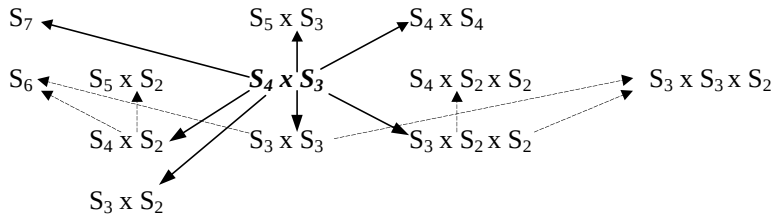

Fig. 12. Possible switches from the attractor with $S_4 \times S_3$ symmetry consequent to different types of perturbation. Solid up-pointing arrows correspond to fusion of nodes. Solid down-pointing arrows correspond to fission of nodes. Dashed up-pointing arrows represent the second step of swapping of a node between clusters.

the basin of this attractor riddles the basin of the other attractor. Once again, the probability of fusion occurring depends upon the density of the basin riddling. In Fig. 12 we show the switches possible for the attractors with $S_4 \times S_3$ symmetry consequent to different types of sensory perturbation (different "odors").

Thus there are several reasons why different perturbations of the same attractor may be associated with different transition probabilities to other attractors. This derives from the structure of phase space in the transverse direction to the invariant manifold and the relationship between the attractor and the perturbation.

4.2. *Transverse Lyapunov exponents and unstable periodic orbits*

The tendency of nodes to coalesce into clusters or desynchronise into individual nodes following perturbation depends upon the behavior of the phase space transverse to the invariant manifolds. Suppose A is an invariant set of the system (6) and an orbit is perturbed some small distance, δ, transverse to A. After n iterations, the amplitude of this displacement will be,

$$d = \delta e^{\lambda_r n} \tag{10}$$

where λ_T, is the called *transverse Lyapunov exponent*. Clearly, in the limit as $n \to \infty$ the amplitude of the displacement will grow or diminish according to the sign of λ_T. If $\lambda_T > 0$ then all perturbations grow and the set A is a saddle. If $\lambda_T < 0$ then, on average, perturbed orbits return to A which is thus an attractor in the full phase space. For an attractor with k clusters, there exits a spectrum of k transverse Lyapunov exponents $\{\lambda_T(1), \lambda_T(2), \ldots, \lambda_T(k)\}$ where $\lambda_T(j)$ describes the growth or decay of perturbations transverse to the invariant manifold containing the jth cluster. In Appendix I, it is shown that with the logistic equation (5) governing the behavior of the local nodes, these are given by

$$\lambda_T(j) = \lim_{n\to\infty} \frac{1}{n} \sum_{t=0}^{n-1} \log |2ux_i(t)(1-e)| \tag{11}$$

where x_i is one of the nodes in the jth cluster. These can be estimated numerically by choosing a typical orbit on A, and a suitable time-scale t', and calculating the *finite-time transverse Lyapunov exponents*,

$$\lambda_T(j) \cong \frac{1}{t'} \sum_{t=0}^{t'-1} \log |2ux_i'(t)(1-e)| \,. \tag{12}$$

By calculating these it is possible to trace the transverse stability of an invariant manifold for different values of c and u. In Fig. 13, we plot the numerator of (12) against the denominator, t, to illustrate the relationship between the stability of A and the nature of the finite-time transverse Lyapunov exponents. Three scenarios are shown with $c = 0.14$, invariant sets with symmetry $S_3 \times S_4$ and different values of u. The finite time transverse Lyapunov exponents are given as the slope of each calculation. For clarity, only the exponent transverse to the 3-node cluster is shown. During the partially ordered phase with $u = 1.675$ the λ_T's are strictly negative (i) and A is an asymptotically stable attractor. In the complex-ordered phase with $u = 1.72$ the finite time λ_T's are negative (ii) if calculated over long periods of time. However, they are often positive over brief time intervals when the system shadows a transversely unstable periodic orbit. In Fig. 13(b) is shown a magnification of (ii) when A is shadowing an unstable period-4 orbit. During this time the

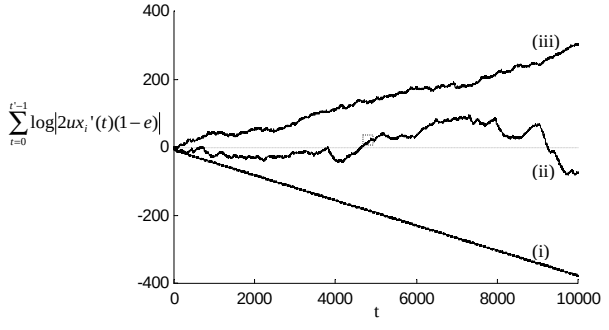

(a)

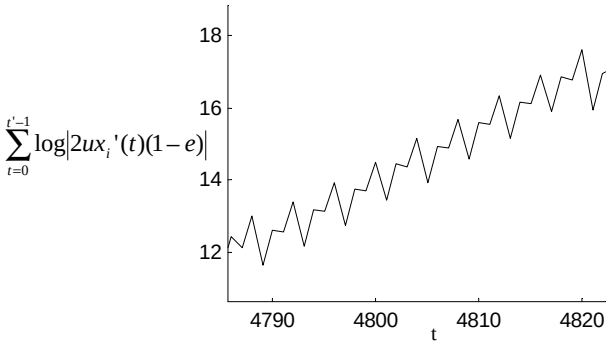

(b)

Fig. 13. Finite-time transverse Lyapunov exponent for the invariant set with $S_3 \times S_4$ symmetry and $c = 0.14$. Vertical axis is calculated along a typical orbit of the system. (a) (i) Asymptotically stable attractor with $u = 1.675$ giving $\lambda_T = -0.0379 < 0$; (ii) Riddled basin attractor with $u = 1.72$ giving $\lambda_T = -0.0076 < 0$; (iii) Saddle set with $u = 1.73$ giving $\lambda_T = 0.030 > 0$. (b) Magnification of scenario (ii) shows the system shadowing a period-4 orbit (for a total of eight complete periods). This graph is contained in the dashed square of (a).

attractor is particularly unstable to any perturbation. Outside of these epochs, the slope is negative and the system is stable. Here A is a riddled basin attractor. For larger values of u the occurrence of unstable epochs increases until one of the λ_Ts becomes positive over long time scales (iii). Hence *all* perturbations transverse to the corresponding invariant manifold grow in amplitude. A has undergone a blowout bifurcation from attractor to saddle.[31]

In Fig. 14, is presented the same transverse Lyapunov exponent for the same attractor with $c = 0.14$ against a range of u. The solid lines gives the average over 60,000 iterations and the dotted lines give the maximum finite-time transverse exponent over intervals of 1000 iterations. From this

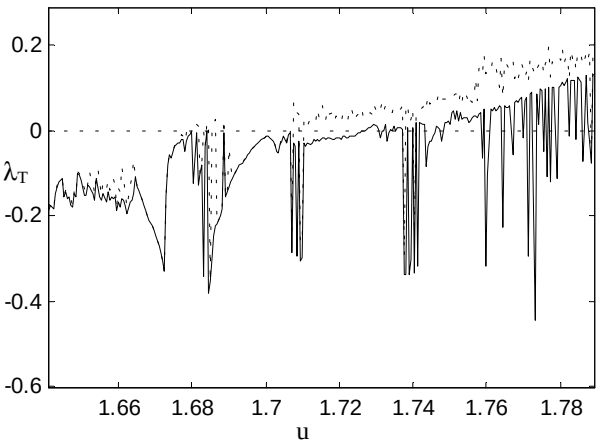

Fig. 14. Transverse Lyaponuv exponent for the 3-node cluster of the attractor [32111], $c = 0.14$ over a range of u. Exponent calculated numerically over 60,000 iterations, after removal of initial transient. Dotted line depicts the maximum of the finite-time Lyapunov exponent over all blocks of 1000 iterations.

graph, we note that when $u < 1.678$, both are negative. This corresponds the region of asymptotically stable attractors. In two regions, ($1.678 < u < 1.688$ and $1.705 < u < 1.727$) the average is negative, but the shorter finite-time exponent is positive. This indicates the existence of riddled basin attractors. For $u > 1.727$ there is a range of values for which the average exponent also becomes positive, corresponding to blowout bifurcations Of note are the multiple windows of asymptotically stable periodic attractors, corresponding to sharp dips in the values of the exponents. This interrupts the gradual increase in the exponents, causing a *blurring* of the blowout bifurcations over a range of parameter values.[27]

4.3. *Anisotropic riddling*

We have already seen that the possible type of attractor switches evoked by transverse perturbations are different to those following perturbations tangeant to invariant manifolds. However, even amongst transverse perturbations, the transition probabilities can be markedly different. This can be true even for clusters of the same size, and reflects the anisotropic nature of basin riddling in high-dimensional systems.[36] For example, there are parameter values for which attractor basins are riddled in one transverse direction, but not in others. Hence if we define $P_R(\delta, s)$

as the probability that the evolution returns to the same attractor following a perturbation of size δ of a specific odor, s, then we may have;

$$s_1 \neq s_2 \Rightarrow P_R(\delta^+, s_1) \neq P_R(\delta^+, s_2) \qquad (13)$$

even if s_1 and s_2 both perturb clusters of the same size. Note that (7) is essentially a period of iterating G in the presence of anisotropic noise. In our model, this derives from the topographic organisation of sensory input from the nasal mucosa.

A final point is that when G is operating in a regime allowing different dynamical archetypes the spectrum of finite-time λ_T's varies markedly. The transition probabilities vary in tandem. This implies that the "state" of the system just prior to sensory stimuli has a significant bearing on the sensory-evoked activity of the model.

4.4. *Heteroclinic connections and networks of attractors*

A perturbation which "knocks" the system out of an invariant subspace in the vicinity of a transversely unstable periodic orbit — where a λ_T is positive — causes it to shadow the unstable manifold of this orbit toward another attractor. Manifolds which are unstable (repelling) for one asymptotic state and stable (attracting) for another are termed *heteroclines*. More formally, we recall that the alpha limit set,

$$\alpha(X) = \bigcap_{N>0} \overline{\bigcup_{n>N} X_{-n}}$$

is the "backwards" asymptotic state of an orbit. If A_1 and A_2 are two disjoint compact invariant sets, then

$$c(A_1, A_2) = \{X \in \Re^N | \alpha(X) \subseteq A_1, \omega(x) \subseteq A_2\},$$

is the set of all heteroclinic connections from A_1 to A_2. It is the structure of these heteroclines that determines how (6) behaves once it has been perturbed off an attractor. Heteroclines can run between conjugate attractors or those on different levels of the isotropy lattice. They may connect a riddled basin attractor to an asymptotically stable attractor, or may interconnect different riddled basin attractors. In the former case, the connection can only be one-way. Otherwise, there may be reciprocal connections. Whereas heteroclinic connections between periodic orbits may be smooth manifolds, those connecting chaotic attractors with riddled basins have a rich algebraic[37] and topological[38] structure which has not yet been fully elucidated. The *strengths* of the interconnections can be estimated by perturbing an attractor according to (7) and numerically calculating the probability of switching to another specific attractor. That is, we can define the average connectivity between two attractors; $Tr(A_1 : A_2, s(t'))$, as the numerically computed *transition probability* from A_1 to A_2 following exposure to an odor, s, for a time sequence t'. The magnitude of the transition probability reflects the density of heteroclines between the two attractors. As for (13) we may have,

$$\begin{aligned} s_1 \neq s_2 \Rightarrow & Tr(A : B, s_1(t')) \\ & \neq Tr(A : B, s_2(t')) \end{aligned} \qquad (14)$$

However, since the exact numeric values of these will vary following a change of variables, they should be treated only as numeric *indicators* of connectivity. We say that a set of attractors $\{A_i\}$ forms a *heteroclinic network of attractors* if for all $i \neq j$,

$$C(A_i, A_j) UC(A_j, A_i) \neq \phi\,.$$

A numeric example of a heteroclinic network is presented in Fig. 15 with $c = 0.12$ and $u = 1.655$. It can be seen that saddles and riddled basin attractors permit large networks of attractors in the complex-ordered phase. Recall that the type of input selects and biases the transitions mediated by the heteroclinic connections. Therefore, such a system is able to switch flexibly and adaptably between coherent states in response to sensory input.

To conclude, the system (6) permits many thousands of attractors in phase space. There are large regions of parameter space where many of these attractors have basins riddled with the basins of other attractors. This leads to large networks of chaotic attractors in phase space, structured by heteroclinic connections between periodic orbits. Due to the anisotropic structure of the basin riddling, different sensory perturbations are associated with different transition probabilities between these attractors. This is the basis by which distinct odors may be perceived differently in the present model of the olfactory bulb.

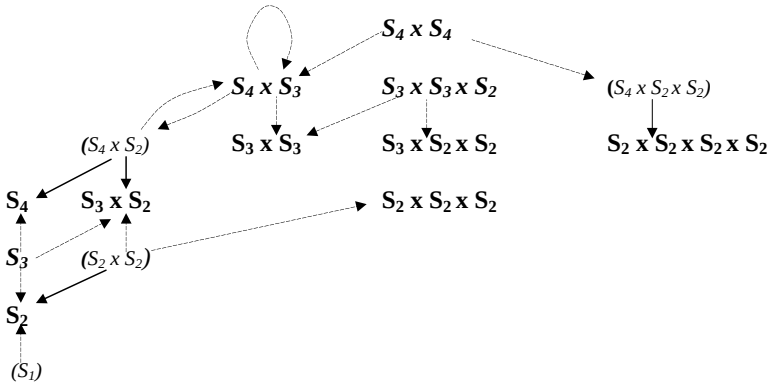

Fig. 15. Heteroclinic network of attractors in the complex phase ($c = 0.12$ and $u = 1.655$). Chaotic saddles are in (*italics*), riddled basin attractors in bold, and asymptotically stable attractors in *bold italics*. Results obtained by finding all invariant sets with a positive measure basin of attraction, and then determining the stability of these by adding small perturbations and inspecting the transverse Lyapunov exponents. Solid lines (exiting saddles) indicate that $Tr(A : B, s) = 100\%$ (for some s); dashed lines, (exiting riddled basin attractors) indicate that $0 < Tr(A : B, s) < 100\%$.

5. The Inspiration-Expiration Cycle: Comparison of the Model with the Experimental EEG

Having described the dynamical properties of our model, we know show how it can reproduce the function and electrophysiology of the olfactory bulb during the inspiration-expiration cycle. Following Kaneko,[12] we propose that the bulb normally operates in the complex-ordered phase. This is achieved through a judicious balance between synaptic connectivity, c and gain, u. It ensures the existence of a very large heteroclinic network of attractors.

5.1. *The normal inspiration-expiration dynamics of the bulb*

A riddled basin attractor with a large basin of attraction achieves the role of the "searching" attractor that appears during expiration. In the complex-ordered phase, attractors with a one or two clusters of synchronised nodes and many unsynchronised nodes have both these properties. An example are the attractors with code [32111]. Such attractors permit different types of transverse and tangential perturbation, allowing a range of transitions according to the nature of the perturbation. Moreover, the pattern of activity of these attractors is irregular and poorly synchronised — precisely the character of the EEG recorded over the bulb during expiration.

At the beginning of inspiration, contact between a specific odorant and receptors in the nasal mucosa leads to excitation of a very small number of sensory neurons. As discussed above, this produces the anisotropic noise modeled by (7), evoking a jump from the searching attractor to a specific robust attractor. This switch serves as the dynamic "fingerprint" for inhalation of that odor, permitting its perception. With basin riddling, this process can occur for even microscopic odor concentrations. If the perturbation is transverse, the attractors permissible include [311111], [221111], [211111], [41111] or conjugate attractors of [32111]. Tangential perturbations allow jumps to attractors further up the isotropy lattice, such as [332] which are possibly better candidates for our model as they typically have periodic or almost-periodic behavior and large clusters of synchronised nodes, thus matching the character of the EEG recorded over the bulb.

As noted in Sec. 3.1, riddled basin attractors in the complex phase typically have large volume, particularly those with many unsynchronised nodes. For example with $c = 0.12$ and $u = 1.689$, numerical simulations indicate that attractors with code [32111] occupy almost 50% of phase space. As noted above, these attractors are therefore selected by isotropic noise. Such noise, present intrinsically in the bulb, is thus required to reinstate the searching attractor prior to the next inhalation. This completes the inhalation-exhalation cycle. Figure 16

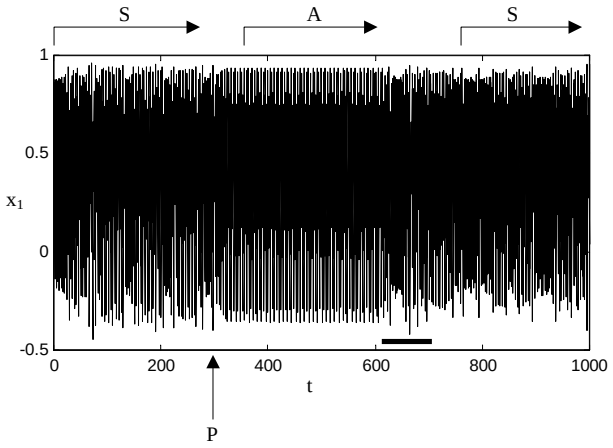

Fig. 16. Simulation example of the inhalation-exhalation cycle in the model bulb. The model has been initiated on a riddled basin attractor with code $[31^5]$, S (the searching attractor). After 300 iterations, a random perturbation, P, of order 10^{-10} has been added for one time step to one of the unsynchronised nodes to simulate odor inhalation. Subsequently, a robust attractor, A, with code $[321^3]$ appears. After 300 iterations, an isotropic noise term of amplitude 0.05 has been added to the system (solid bar). This causes the system to return to the searching attractor, S.

depicts an example of such a cycle. The model has been initiated on a riddled basin attractor, then perturbed at "P" by a simulated odor (of amplitude 10^{-10}). This causes the system to jump onto a robust attractor, as evidenced by the appearance of regular behavior. At the end of "inspiration", a short burst of low amplitude noise has been added to the system. Consequently the riddled basin attractor has reappeared: The bulb is ready for the next odor. For clarity, only the behavior of one node has been presented.

5.2. *Abnormal dynamics associated with hallucinations*

We finish with a note on the occurrence of olfactory hallucinations. *Hallucinations* are perceptual experiences that occur in the absence of sensory stimuli. In the context of the present model, this corresponds to a *spontaneous* jump from the searching attractor onto a asymptotically stable attractor. Olfactory hallucinations occasionally occur prior to some forms of seizures,[39] after ingestion of psychostimulants such as amphetamines, and in some instances of schizophrenia.[40] Seizures are associated with the occurrence of highly synchronised periodic-like behavior in large numbers of neurons.[39] The aetiology of at least some seizures involves a deficit in the function of inhibitory interneurons.[41] In our model, this implies a change of the parameter u, possibly to a periodic window for the dynamics of the searching attractor. Thus, the olfactory bulb would be captured by a robust, large volume attractor, severely disrupting the normal dynamics of the bulb. This would explain the unpleasant and often unusual nature of these phenomena.

Synaptic responsiveness in the brain is modified by diffusely projecting neurons whose cell bodies are found in subcortical nuclei such as the locus ceruleus and dorsal raphe nucleus.[25] These neurons, which project strongly to the olfactory bulb, function by releasing monoamine neurotransmitters such as dopamine, noradrenaline and serotonin. The synaptic modulatory effects of these monoamines is facilitated by a second messenger system.[25] Ingestion of amphetamine (a dopamine/noradrenaline agonist) or LSD (a serotonin agonist) leads to alteration of synaptic coupling strength by disrupting these monoamine pathways. Thus we model amphetamine/LSD ingestion as an abnormal tuning of the parameter, c. This results in a change in the stability of attractors and the strengths of their connections. If the searching attractor underwent a blowout bifurcation, then the system would jump to an attractor in the transverse direction that first lost stability. This would explain the intrusiveness of substance-induced hallucinatory experiences and their persistence over a period of hours.

Although the aetiology of schizophrenia is still unclear, the mechanism of hallucinations is possibly similar to those of amphetamine/LSD psychosis: Anti-psychotic medications typically target monoamine neurotransmitters[25,40] and studies have found abnormal distributions of monoamine neuro-receptors in the brains of subjects with schizophrenia.[42] Therefore, hallucinations in schizophrenia are also modeled as detuning the coupling parameter c into a region where the searching attractor has become a saddle.

These final notes are meant as conjectures only, although they serve to illustrate the potential clinical utility of the present model and the advantage of giving a concept such as "perception" an

explicit definition within the framework of a neural model.

6. Discussion: Strengths, Weaknesses and Future Directions

This paper proposes a nonlinear model of perceptual dynamics in the olfactory bulb that explains its ability to discriminate between many thousands of different odors, present in possibly very small concentrations. Essentially we illustrate a proposal by Kaneko[12] concerning the potential role of riddled basin attractors in Freeman's[8,33] description of olfactory bulb dynamics. In addition, we utilise a group-theoretic ordering of the dynamics, the isotropy lattice, based on the symmetries of the attractors. The topographic organisation of sensory input is introduced and the model is able to replicate the discriminatory function of the bulb during the normal cycle of inspiration-expiration. For pathological values of either the coupling or the gain parameter, our model "hallucinates".

There are several links between the behavior of the model and neurophysiology, that are worth noting:

1. The spatio-temporal behavior of the model is consistent with the character of the EEG recorded over the bulb. That is, during exhalation, the behavior is discordant and chaotic. Following inhalation of an odor, it switches to a periodic or almost-periodic signal with a pattern of spatial coherence specific to the odor.
2. Synchronous oscillations play a central role in our model. The number and size of clusters of synchronised nodes distinguishes attractors, determines the invariant manifolds that contain them, and thus the transverse stability. There is currently very active neuroscientific research devoted to the role of synchronous oscillations in normal[43–46] and disturbed[47] brain function, particularly in regard to the perception of sensory stimuli. This paper proposes a mechanism and role for synchronous oscillations in neural systems and is thus relevant to this research.
3. A feature of the model is its ability to produce quite complex behavior. Some attractors display spontaneous jumps amongst a number of dynamical archetypes, each associated with different transverse stability. The response of these attractors to sensory stimulation thus depends strongly on the dynamics prior to the stimulus. This is also consistent with neurophysiology research suggesting that behavioral and neurophysiological consequences of sensory input are strongly influenced by prestimulus brain state as reflected in the prestimulus EEG.[48–50]

Introducing the algebraic classification of attractors and transverse Lyapunov exponents into the discussion of the model's behavior permits a degree of formal analysis. This complements investigations based almost solely on numerical simulations of neural systems exhibiting synchronous chaos.[51] Numerical simulations of nonlinear and iterated functions are particularly susceptible to a number of systematic errors. For example, spurious synchronisation can result from rounding error, and binary floating-point arithmetic can cause spurious desynchronisation. Therefore, complementing analytic and numeric techniques is desirable. However, there are several significant simplifications which were required to make the analysis more tractable:

1. The coupling strengths and local dynamics within all nodes are symmetric. The symmetry forces the existence of invariant subspaces, which are central to our discussion. However, breaking these symmetries, by relaxing the constraints on either the local dynamics or coupling strengths, leaves much of the qualitative features of the dynamics intact.[52] Breaking the symmetry by a small amount is essentially the same as adding a small amplitude noise signal to (7). Symmetries in such circumstances can be detected by studying the statistical correlations between the individual nodes.[53]
2. The approximation of local neural dynamics by (1) assumes that neural behavior is solely determined by neural interactions, and ignores other contributions, such as leaky membrane channels and the resting membrane potential. The restrictions on excitatory-inhibitory interactions which allow substitution of (1) by (4) and (5) effectively limit our description to a

cross-section of the original parameter space. Nonetheless, the behavior exhibited is adequate to fulfil our original aims and replicate the EEG. Preliminary numerical simulations of (1) indicate similar dynamics for a variety of parameter values.

3. The dimensionless units of the governing equations prohibit incorporation of physiological parameters and thus explicit hypothesis testing. However, qualitative considerations, as discussed in Sec. 5.2, are still possible. Moreover, it is generally accepted that even in networks like the olfactory bulb, physiological measurements have large errors, restricting precise quantitative analysis.

Thus analytic approaches have the advantage of rigor but are limited by simplifications. Conversely, physiological realism often leads to reliance on numerics with its various pitfalls. The convergence of analytic, numeric and experimental research constitutes a strong argument for the role in brain function of nonlinear systems with partial synchronisation and partial stability.

Improving the current model can be achieved by replacing the coupling parameter, c, with the $N \times N$ *connection matrix*[54] $C = [c_{ij}]$, where c_{ij} is the synaptic connectivity from node i to node j. Firstly, this permits introduction of patterns of interconnection with a neurohistological character[55] such as clustering, strong reciprocity,[56] and "small world" networks.[57] The symmetry of C is broken, although in a particular manner that leaves less symmetric relations intact. Secondly, it is possible to introduce a learning rule which allows the dynamical formation of Hebbian assemblies.[58] This involves the strengthening of effective synaptic connectivity between cells which fire synchronously,[59] leading to assemblies of preferentially interconnected neurons within the network. This principle has been proposed as a mechanism of learning of odors in the olfactory bulb.[8] It can be introduced parsimoniously into the current model by updating each c_{ij} following inhalation of any odor which was paired with a "conditioned stimulus". Coupling between nodes with very small average Euclidean separation is strengthened, whereas those with large separation are weakened. If the increment is small then note (1) above, holds.

Given the modular structure of the cerebral cortex, it is possible that similar models may have some application to understanding the neural dynamics at the scale of the whole brain. Thus dynamics involving riddled basins and heteroclinic networks may underlie other brain functions, such as visual and auditory perception, learning[60] and computation.[22,61,62]

Acknowledgments

The author is very grateful to P. Ashwin and M. Nichol for many fruitful discussions, and to P. Ashwin for helpful comments on the manuscript. M. B. is the recipient of a University of Sydney Postgraduate cholarship and a Travel Research Grant from the Faculty of Medicine, the University of Sydney.

Appendix I

Basic group theoretic definitions

A non-empty set, $\Gamma = \{\gamma_i\}$, together with an operation, $\bullet$, is called a group if it satisfies the following;

(i) Γ is *closed* under the action of $\bullet$. That is for any two elements γ_i, $\gamma_j \in \Gamma$, there exists $\gamma_k \in \Gamma$ such that $\gamma_i \bullet \gamma_j = \gamma_k$.
(ii) $\gamma_i, \gamma_j, \gamma_k \in \Gamma$ implies that $(\gamma_i \bullet \gamma_j) \bullet \gamma_k = \gamma_i \bullet (\gamma_j \bullet \gamma_k)$.
(iii) For all $\gamma_i \in \Gamma$, there exists an *identity element* denoted e such that $\gamma_i \bullet e = e \bullet \gamma_i = \gamma_i$.
(iv) For all $\gamma_i \in \Gamma$ there exists an *inverse*, $\gamma_i^{-1} \in \Gamma$ such that $\gamma_i \bullet \gamma_i^{-1} = \gamma_i^{-1} \bullet \gamma_i = e$.

Examples of groups of infinite size include the integers under the action of addition. Finite groups of size n include the integers modulus n under the action of addition. The set of permutations of n objects is also a finite group and is called the symmetry group, S_n.

A *subgroup* Σ of Γ is any subset of Γ which is also a group. For example, the even integers under the action of addition is a subgroup of the integers. Two subgroups Σ and Σ' are said to be *conjugate* ($\Sigma \sim \Sigma'$) if there exists $\gamma \in \Gamma$ such that $\Sigma' = \gamma^{-1}\Sigma_\gamma$. A *proper subgroup* $\Sigma < \Gamma$ of Γ is a subgroup that is strictly smaller that Γ.

The isotropy subgroups and fixed point subspace of a subgroup are defined in the main text. Note that

the fixed point subspaces of the group are quite different from the fixed points of the map G (although every fixed point of G will be contained within some fixed point subspace). It can be shown that conjugate subgroups have fixed point subspaces that are mapped onto each other by the group. More precisely,[36] for any isotropy subgroup $\Sigma \subseteq \Gamma$ and any $\gamma \in \Gamma$ then $\gamma^{-1}\Sigma_\gamma$ is an isotropy subgroup and,

$$\mathrm{Fix}(\gamma^{-1}\Sigma_\gamma) = \gamma^{-1}\mathrm{Fix}(\Sigma)\,.$$

Hence congugate attractors are mapped onto each other by the symmetries of the whole system, G.

Appendix II

Derivation of the transverse Lyapunov exponent

Suppose A is an invariant set of the system G and an orbit of A is perturbed some small distance, δ, transverse to A. After n iterations of G, the amplitude of this displacement will be,

$$d = \delta e^{\lambda_T n} \tag{A1}$$

where λ_T, is the transverse Lyapunov exponent. We can derive λ_T by taking a change of variables and linearising G in the neighborhood of the invariant manifold. Consider a synchronised cluster containing two nodes, x_1 and x_2. Taking a change of variables,

$$\begin{aligned} y(t) &= x_1(t) + x_2(t) \\ z(t) &= x_1(t) - x_2(t)\,, \end{aligned} \tag{A2}$$

we see that $y(t)$ describes the behavior within the cluster and $z(t)$ describes any displacement in the transverse direction. Then by substituting (A2) into (6), taking the Taylor series expansion around $z = 0$ and dropping higher-order terms we obtain,

$$z(t+1) = Df_y(1-e)z(t)\,, \tag{A3}$$

where Df_y is the derivative of f with respect y. Hence, after n iterates the transverse displacement will be,

$$\begin{aligned} d = z(n) &= z(0)\prod_{t=1}^{n} Df_y(1-e)\,, \\ &= \delta \prod_{t=1}^{n} Df_y(1-e)\,. \end{aligned} \tag{A4}$$

Taking the logarithm of both sides we obtain,

$$\lambda_t = \lim_{n\to\infty} \frac{1}{n}\sum_{t=1}^{n} \log|Df_y(1-e)|\,. \tag{A5}$$

If we restrict ourselves now to orbits on the invariant set, A, then $x_1(t) = x_2(t)$. Thus, substituting the logistic map and x_1 into (A4),

$$\lambda_t = \lim_{n\to\infty} \frac{1}{n}\sum_{t=1}^{n} \log|2ux_1(t)(1-e)|\,. \tag{A6}$$

The convergence of this calculation to the same value for different orbits on A requires that all orbits on A are typical (i.e., A supports an *ergodic* invariant measure). Then we can obtain a numeric approximation for λ_T for some finite (large) T number of iterations of a single orbit $\{x_1(0), x_1(1), \ldots, x_1(T)\}$ on the attractor. The assumption that A supports an ergodic measure can be checked by ensuring this value converges to the same value for increasing T and different orbits of A.

References

1. G. Shephard 1988, "Chemical senses," *Neurobiology* (Oxford University Press, Oxford).
2. M. Bear, B. Connors and M. Paradiso 1996, "Chemical senses," *Neuroscience* (Williams and Wilkins, Baltimore).
3. J. Dodd and V. Castellucci 1991, "Smell and taste: The chemical senses," *Principles of Neural Science*, ed. E. Kandall and Schwarz (Publisher, City).
4. R. Reed 1990, "How does the nose know?" *Cell* **60**, 1–2.
5. W. Freeman 1987, "Techniques used in the search for the physiological basis of the EEG," *Handbook of Electroencephalography and Clinical Neurophysiology*, ed. A. Gevins and A. Remond (Elsevier, London).
6. W. Freeman and G. Viana Di Prisco 1986, "EEG spatial patterns differences with discriminated odors manifest chaotic and limit cycle attractors in olfactory bulb of rabbits," *Brain Theory*, ed. G. Palm (Springer-Verlag, London).
7. W. Freeman and W. Schneider 1982, "Changes in spatial patterns of rabbit olfactory EEG with conditioning to odors," *Psychophysiology* **19**, 44–56.
8. C. Skarda and W. Freeman 1987, "How brains make chaos in order to make sense of the world," *Behav. Brain Sci.* **10**, 161–195.
9. W. Freeman 1991, "The physiology of perception," *Scientific American* **264**, 78–85.

10. J. Kauer 1991, "Contributions of topography and parallel processing to odor coding in the vertebrate olfactory pathway," *Trends Neurosci.* **14**, 79–85.
11. K. Kaneko 1998, "On the strength of attractors in a high-dimensional system," *Physica* **D124**, 322–344.
12. K. Kaneko 1997, "Dominance of Milnor attractors and noise-induced selection in a multiattractor system," *Phys. Rev. Lett.* **78**, 2736–2739.
13. K. Kaneko 1992, "Overview of coupled map lattices," *Chaos* **2**, 279–282.
14. J. Milnor 1985, "On the concept of attractor," *Commun. Math. Phys.* **99**, 177–195.
15. P. Nunez 1992, *Neocortical Dynamics and Human EEG Rhythms* (Oxford University Press, Oxford).
16. M. Freeman 1975, *Mass Action in the Nervous System* (Academic Press, New York).
17. P. Robinson, C. Rennie and J. Wright 1997, "Propagation and stability of waves of electrical activity in the cerebral cortex," *Phys. Rev.* **E56**, 826–841.
18. X. Wang 1991, "Period-doublings to chaos in a simple neural network: An analytic proof," *Complex Systems* **5**, 425–441.
19. A. Minai and T. Anand 1998, "Chaos-induced synchronisation in discrete-time oscillators driven by a random signal," *Phys. Rev.* **E57**, 1559–1562.
20. P. Collet and J. Eckmann 1980, *Iterated Maps on the Interval as Dynamical Systems* (Birkhauser).
21. S. Van Strien 1988, "Smooth dynamics on the interval," in *New Directions in Dynamical Systems* (Cambridge University Press, Cambridge).
22. K. Kaneko 1994, "Information cascade with marginal stability in a network of chaotic elements," *Physica* **D77**, 456–472.
23. A. Tabarov, Y. Maistrenko and E. Mosekilde 2000, "Partial synchronisation in a system of coupled logistic maps," *Int. J. Bif. Chaos* **10**, 1051–1066.
24. R. Mendes 1999, "Clustering and synchronization with positive Lyaponuv exponents," *Phys. Lett.* **A257**, 132–138.
25. J. Cooper, F. Bloom and R. Roth 1991, *The Biochemical Basis of Neuropharmacology* (Oxford University Press, Oxford).
26. P. Ashwin and J. Terry 2000, "On riddling and weak attractors," *Physica* **D142**, 87–100.
27. P. Ashwin, E. Covas and R. Tavakol 1999, "Transverse instability for non-normal parameters," *Nonlinearity* **12**, 563–577.
28. E. Barreto, B. Hunt, C. Greborgi and J. Yorke 1997, "From high dimensional chaos to stable periodic orbits: The structure of parameter space," *Phys. Rev. Lett.* **78**, 4561–4564.
29. J. Alexander, J. Yorke, Z. You and I. Kan 1992, "Riddled basins," *Int. J. Bif. Chaos* **2**, 795–813.
30. Y. Maistrenko, V. Maistrenko, A. Popovich and E. Mosekilde 1998, "Transverse instability and riddled basins in a system of two coupled logistic maps," *Phys. Rev.* **E57**, 2713–2732.
31. P. Ashwin, J. Buescu and I. Stewart 1996, "From attractor to chaotic saddle a tale of transverse instability," *Nonlinearity* **9**, 703–37.
32. P. Ashwin and J. Swift 1992, "The dynamics of n-weakly coupled identical oscillators," *J. Nonlinear Sci.* **2**, 69–108.
33. W. Freeman 1987, "Simulation of chaotic EEG patterns with a dynamic model of the olfactory system," *Biol. Cybern.* **56**, 139–150.
34. P. Ashwin 1995, "Attractors stuck on to invariant subspaces," *Phys. Lett.* **A209**, 338–344.
35. E. Stone and A. Cutler 1996, "Archetypal analysis of spatio-temporal dynamics," *Physica* **D90**, 209–224.
36. P. Ashwin and M. Breakspear 2000 "Anisotropic properties of riddled basins," *Physics Letters* **A280**, 139–145.
37. P. Ashwin and M. Field 1999, "Heteroclinic networks in coupled cell systems," *Arch. Rational Mech. Anal.* **148**, 107–143.
38. J. Eckmann and D. Ruelle 1984, "Ergodic theory of chaos and strange attractors," *Rev. Modern Phys.* **57**, 617–653.
39. T. Pedley 1984, "Epilepsy and the human electroencephalogram," in *Electrophysiology of Epilepsy*, ed. P. Schwartzkroin and H. Wheal (Academic Press, London).
40. P. McKenna 1997, *Schizophrenia and Related Syndromes* (Psychology Press, Hove).
41. W. Spencer and E. Kandel 1969, "Synaptic inhibition in seizures," in *Basic Mechanisms of the Epilepsies*, ed. H. Jasper, A. Ward and A. Pope (Little, Brown and Company, Boston).
42. A. Bleich, S. Brown, R. Kahn and H. van Praag 1988, "The role of serotonnin in schizophrenia," *Schiz. Bull.* **14**, 297–315.
43. C. Gray, P. Konig, A. Engel and W. Singer 1989, "Oscillatory responses in cat visual cortex exhibit inter-columnar synchronization which reflects global stimulus properties," *Science* **338**, 334–337.
44. M. Stopfer, S. Bhagavan, B. Smith and G. Laurent 1997, "Impaired odor discrimination on desynchronization of odor-encoding neural assemblies," *Nature* **390**, 70–74.
45. W. Miltner, C. Braun, M. Arnold, H. Witte and E. Taub 1999, "Coherence of gamma-band EEG activity as a basis for associative learning," *Nature* **397**, 434–436.
46. E. Rodriguez, N. George, N. Lachaux, J. Martinerie, B. Renault and F. Varela 1999, "Perception's shadow: Long-distance synchronization of human brain activity," *Nature* **397**, 430–433.
47. A. Haig, E. Gordon, V. De Pascalis, R. Meares, H. Bahramali and A. Harris 2000, "Gamma activity in schizophrenia: Evidence of impaired network binding?" *Clin. Neurophysiol.* **111**, 1461–1468.
48. M. Brandt, B. Jansen and J. Carbonari 1991, "Pre-stimulus EEG patterns and visual evoked

response," *Electroenceph. and Clin. Neurophysiol.* **80**, 16–20.
49. E. Rahn and E. Basar 1993, "Prestimulus EEG-activity strongly influences the auditory evoked vertex response," *Int. J. Neuroscience* **69**, 207–220.
50. A. Haig and E. Gordon 1998, "Prestimulus EEG alpha phase synchronicity influences N100 amplitude and reaction time," *Psychophysiol.* **35**, 591–595.
51. D. Hansel 1996, "Synchronised chaos in local cortical circuits," *Int. J. Neural Sys.* **7**, 403–415.
52. P. Buono, M. Golubitsky and A. Palacios 2000, "Heteroclinic cycles in rings of coupled cells," *Physica* **D143**, 74–108.
53. P. Schneider and P. Grassberger 1997, "Studying attractor symmetries by means of cross-correlation sums," *Nonlinearity* **10**, 749–762.
54. T. Sejnowski 1976, "On global properties of neuronal interactions," *Biol. Cybern.* **22**, 85–95.
55. R. Kotter and F. Sommer 2000, "Global relationship between anatomical connectivity and activity propagation in the cerebral cortex," *Phil. Trans. R. Soc. Lond.* **355B**, 127–134.
56. K. Friston, G. Tononi, O. Sporns and G. Edleman 1995, "Characterising the complexity of neuronal interactions," *Human Brain Mapp.* **3**, 302–314.
57. D. Watts and S. Strogatz 1998, "Collective dynamics of small world networks," *Nature* **393**, 440–442.
58. D. Hebb 1949, "The first stage of perception," reprinted in *Brain Function*, ed. G. Shaw and G. Palm (World Scientific, Singapore).
59. Y. Hayakawa and Y. Sawada 2000, "Learning-induced synchronisation of a globally coupled excitable map system," *Phys. Rev.* **E61**, 5091–5097.
60. H. Nakajimi and Y. Ueda 1996, "Riddled basins of the optimal states in learning dynamical systems," *Physica* **D99**, 35–44.
61. S. Sinha and W. Ditto 1998, "Dynamics based computation," *Phys. Rev. Lett.* **81**, 2156–2159.
62. I. Tsuda 2001, "Towards on interpretation of dynamic neural activity in terms of chaotic dynamical systems," *Behav. Brain Sci.* **24** (to appear).